

Nonlinear dynamic analysis of a relatively short spherical gas journal bearing system[†]

Cheng-Chi Wang^{1,*} and Chao-Lin Kuo²

¹Department of Mechanical Engineering, Far East University, Tainan, Taiwan

²Institute of Maritime Information and Technology, National Kaohsiung Marine University, Kaohsiung, Taiwan

(Manuscript Received June 3, 2009; Revised January 20, 2010; Accepted May 1, 2010)

Abstract

This paper studies the nonlinear dynamic behavior and bifurcation of a rigid rotor supported by two relatively short spherical gas journal bearings. The modified Reynolds equation is solved by a hybrid numerical method combining the differential transformation method (DTM) and the finite difference method (FDM). The analytical results reveal a complex dynamic behavior comprising periodic, sub-harmonic and quasi-periodic responses as the rotor mass and bearing number are increased. The results obtained using the hybrid DTM&FDM scheme are found to be in good agreement with those of a hybrid scheme comprising the successive over relaxation (SOR) method and the FDM scheme. Therefore, the DTM&FDM method provides an effective means of gaining insights into the nonlinear dynamics of relatively short spherical gas rotor-bearing systems.

Keywords: Bifurcation; Relatively short spherical gas bearing; Differential transformation method; Successive over relaxation

1. Introduction

Gross [1] developed perturbation solutions for steady, self-acting, infinitely long journal and plane wedge films and showed that the solutions were valid for all ranges of the geometrical parameters. Nikolajsen & Holmes [2] observed non-synchronous vibrations in a flexible, symmetric rotor supported on two identical plane journal bearings by centralized squeeze film dampers. Li & Taylor [3] observed sub-harmonic motions in rotor-bearing systems. Ehrich [4] discussed the appearance of 8th and 9th order sub-harmonic vibration in a turbomachine.

Zhao et al. [5] investigated the sub-harmonic and quasi-periodic motions of an eccentric squeeze film damper-mounted rigid rotor system. The authors noted that for large values of the rotor unbalance and static misalignment, the sub-harmonic and quasi-periodic motions generated at speeds of more than twice the system critical speed were bifurcated from the unstable harmonic solution. Citing theoretical and experimental evidence, Adiletta et al. [6] reported that a rigid rotor supported by short bearings behaved with sub-harmonic, quasi-periodic or chaotic motion depending on the values of the system parameters. Wang [7-9] presented a series of nu-

merical investigations into the dynamic behavior of different gas journal bearing systems as a function of the rotor mass and the bearing number, respectively.

The present study conducts a numerical investigation into the nonlinear dynamic behavior and bifurcation of a rigid rotor supported by two relatively short spherical gas journal bearings. The remainder of this paper is organized as follows. Section 2 develops a mathematical model describing the time-dependent motions of the center of the rigid rotor. Section 3 develops a hybrid method combining the FDM and the DTM to obtain the required solutions. Section 4 compares the solutions obtained from the DTM&FDM method for the orbits of the rotor center at different values of the rotor mass and rotational speed with those obtained using a hybrid scheme comprising the SOR method and the FDM scheme. The DTM&FDM method is then used to analyze the vibrations of the rotor center at various values of the rotor mass and bearing number, respectively. Finally, Section 5 draws some brief conclusions.

2. Mathematical modeling

In developing the spherical gas journal bearing model considered in this study, it is assumed that the gas flow is isothermal and the gas viscosity is constant. The pressure distribution in the gas film between the shaft and the bushing is modeled by the Reynolds' equation, i.e.

[†]This paper was recommended for publication in revised form by Associate Editor Eung-Soo Shin

*Corresponding author. Tel.: +886 6 5979566, Fax: +886 6 5977115

E-mail address: wccipn@yahoo.com.tw

© KSME & Springer 2010

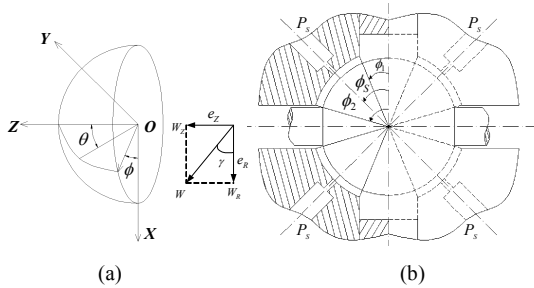


Fig. 1. Cross section of a relatively short spherical gas film journal bearing.

$$\begin{aligned} \csc \phi \frac{\partial}{\partial \phi} \left(\frac{1}{\csc \phi} p h^3 \frac{\partial p}{\partial \phi} \right) + \csc^2 \phi \frac{\partial}{\partial \theta} \left(p h^3 \frac{\partial p}{\partial \theta} \right) = \\ A_s \frac{\partial}{\partial \phi} (p h) + \sigma \frac{\partial}{\partial \tau} (p h) \end{aligned} \quad (1)$$

where p is the dimensionless pressure corresponding to the atmospheric pressure, P_a ; h is the dimensionless gap between the rotating shaft and the bushing, i.e. the radial clearance, C_r ; and μ is the gas viscosity. The bearing system is modeled using the spherical coordinate system shown in Fig. 1, in which the position of any point is defined in terms of its radial distance from the origin, its zenith angle θ from the positive z-axis, and its azimuth angle ϕ from the positive x-axis.

Since the current analysis considers a relatively short spherical gas journal bearing model, the first term on the left-hand side of Eq. (1) can be neglected. Equation (1) can therefore be simplified as

$$\csc^2 \phi \frac{\partial}{\partial \theta} \left(p h^3 \frac{\partial p}{\partial \theta} \right) = A_s \frac{\partial}{\partial \phi} (p h) + \sigma \frac{\partial}{\partial \tau} (p h) \quad (2)$$

The gas film pressure distribution satisfies the following boundary conditions:

(a) The gas pressure at $\phi = \phi_1$ and $\phi = \phi_2$ is equal to the atmospheric pressure P_a .

(b) The gas pressure P varies as a periodic function of θ .

The analysis presented in this paper considers the rotor-bearing system to be comprised of a perfectly balanced rigid rotor of mass m_r , supported symmetrically on two identical relatively short journal bearings, mounted in turn on rigid pedestals. It is further assumed that during the entire rotation, the rotor and bearing axes remain aligned at all times. Thus, the analysis problem can be reduced to that of a single bearing supporting a rotating rotor of mass m_r with two degrees of translatory oscillation in the transverse plane (see Fig. 1).

In the transient state, the equation of motion of the journal can be written as

$$m_r \ddot{X}^* + F_{gk}^* = F_{elx}^*, \quad (3)$$

$$m_r \ddot{Y}^* + F_{gfy}^* = F_{ely}^* \quad (4)$$

in which F_{elx}^* and F_{ely}^* are the components of the external loading.

3. Mathematical formulation of hybrid method

3.1 Hybrid method comprising SOR method and finite difference method (SOR&FDM)

In solving the Reynolds equation, Eq. (2) is discretized using the central-difference scheme in the θ and ϕ directions and the implicit-back-difference scheme in time τ . Note that for simplicity, the discretization process is performed using a uniform mesh size. If Eq. (2) is solved directly, there will be a total of five unknowns. Accordingly, in this hybrid method, the Reynolds equation is solved using the SOR method [9] since its use reduces the number of unknowns from five to three.

3.2 Hybrid method comprising differential transformation method and finite difference method (DTM&FDM)

Differential transformation is one of the most widely used techniques for solving differential equations due to its rapid convergence rate and minimal calculation error. A further advantage of this method over the integral transformation approach is its ability to solve nonlinear differential equations [10]. In solving the Reynolds equation for the relatively short spherical gas journal bearing model shown in Fig. 1, the first term on the left-hand side of Eq. (1) can be neglected. So, Eq. (1) becomes Eq. (2) and then Eq. (2) is transformed as:

$$\csc^2 \phi \frac{\partial}{\partial \theta} \left(\frac{1}{2} h^3 \frac{\partial (p^2)}{\partial \theta} \right) = A_s \frac{\partial p}{\partial \phi} h + A_s \frac{\partial h}{\partial \phi} p + \sigma \frac{\partial p}{\partial \tau} h + \sigma \frac{\partial h}{\partial \tau} p \quad (5)$$

Then differentiate the left term of Eq. (5):

$$\begin{aligned} & \csc^2 \phi (3h^2) \frac{\partial h}{\partial \theta} \frac{\partial (p^2)}{\partial \theta} + \csc^2 \phi \frac{\partial^2 (p^2)}{\partial \theta^2} h^3 \\ &= 2A_s \frac{\partial p}{\partial \phi} h + 2A_s \frac{\partial h}{\partial \phi} p + 2\sigma \frac{\partial p}{\partial \tau} h + 2\sigma \frac{\partial h}{\partial \tau} p \end{aligned} \quad (6)$$

Take differential transformation with respect to the time domain τ and hence Eq. (6) becomes:

$$\begin{aligned} & \csc^2 \phi \otimes 3I \otimes \frac{\partial H}{\partial \theta} \otimes \frac{\partial Q}{\partial \theta} + \csc^2 \phi \otimes J \otimes \frac{\partial^2 Q}{\partial \theta^2} = 2A_s \frac{\partial P}{\partial \phi} \otimes H \\ &+ 2A_s \frac{\partial H}{\partial \phi} \otimes P + 2\sigma \frac{\partial P}{\partial \tau} \otimes H + 2\sigma \frac{\partial H}{\partial \tau} \otimes P \end{aligned} \quad (7)$$

where

$$Q(k) = P^2 = P \otimes P = \sum_{l=0}^k P_{i,j}(k-l)P_{i,j}(l) \quad (8)$$

$$I(k) = H^2 = H \otimes H = \sum_{l=0}^k H_{i,j}(k-l)H_{i,j}(l) \quad (9)$$

$$\begin{aligned} J(k) &= H^3 = H \otimes H \otimes H \\ &= \sum_{l=0}^k H_{i,j}(k-l) \sum_{m=0}^l H_{i,j}(l-m)H_{i,j}(m) \end{aligned} \quad (10)$$

Having transformed the Reynolds equation in the time do-

Table 1. Comparison of rotor center orbit data calculated by SOR and DTM methods.

	X		Y	
	$\tilde{H} = 0.001$	$\tilde{H} = 0.001$	$\tilde{H} = 0.001$	$\tilde{H} = 0.001$
SOR& FDM $m_r=3.47$	-0.61435590	-0.61435389	-0.42864294	-0.42869027
DTM& FDM kg	-0.61430748	-0.61435069	-0.42869028	-0.42861435
SOR& FDM $A=2.26$	0.599632915	0.599651569	-0.13112036	-0.13118257
DTM& FDM	0.599664340	0.599698823	-0.13112446	-0.13117003

Table 2. Comparison of Poincaré map data for rotor centers computed using different values of time step \tilde{H} .

Rotor mass $m_r = 2.1$ kg			Bearing number $A = 1.2$		
\tilde{H}	X (n T)	Y (n T)	\tilde{H}	X (n T)	Y (n T)
$\pi/300$	-0.63113136	-0.44087269	$\pi/300$	-0.74812268	-0.30840654
$\pi/600$	-0.63114315	-0.44081366	$\pi/600$	-0.74816034	-0.30845706

main, the finite difference method is then used to discretize Eq. (9) with respect to the θ and ϕ directions. Note that Eq. (9) is discretized using the second-order-accurate central-difference scheme for both the first and the second derivatives.

Substituting Eqs. (8-10) into Eq. (7) yields

$$\begin{aligned}
 & + 3 \cdot \csc^2(i\Delta\phi) \cdot \sum_{l=0}^k I_{i,j}(k-l) \sum_{m=0}^l \left[\frac{(H_{i,j+l}(l-m) - H_{i,j-l}(l-m))}{2\Delta\theta} \right] \\
 & \left(\frac{Q_{i,j+l}(m) - Q_{i,j-l}(m)}{2\Delta\theta} \right) \\
 & + \csc^2(i\Delta\phi) \cdot \sum_{l=0}^k J_{i,j}(k-l) \cdot \left[\frac{Q_{i,j+l}(l) - 2 \cdot Q_{i,j}(l) + Q_{i,j-l}(l)}{(\Delta\theta)^2} \right] \quad (11) \\
 & = 2A \cdot \sum_{l=0}^k \left[\left(\frac{P_{i+1,j}(k-l) - P_{i-1,j}(k-l)}{2\Delta\phi} \right) \cdot H_{i,j}(l) \right] \\
 & + 2A \cdot \sum_{l=0}^k \left[\left(\frac{H_{i+1,j}(k-l) - H_{i-1,j}(k-l)}{2\Delta\phi} \right) \cdot P_{i,j}(l) \right] \\
 & + 2\sigma \cdot \sum_{l=0}^k \left[\left(\frac{l+1}{\tilde{H}} \right) P_{i,j}(k-l) \cdot H_{i,j}(l+1) \right] \\
 & + 2\sigma \cdot \sum_{l=0}^k \left[\left(\frac{l+1}{\tilde{H}} \right) H_{i,j}(k-l) \cdot P_{i,j}(l+1) \right]
 \end{aligned}$$

From Eq. (11), $P_{i,j}(k)$ is obtained for each time interval, where i and j indicate the node position and k indicates the k th term.

4. Results and discussions

4.1 Hybrid method comprising SOR method and finite difference method (SOR&FDM)

Table 1 compares the results obtained by the SOR&FDM and DTM&FDM methods for the orbits of the rotor center. It is observed that a good agreement exists between the two sets of results at different values of the rotor mass and rotational

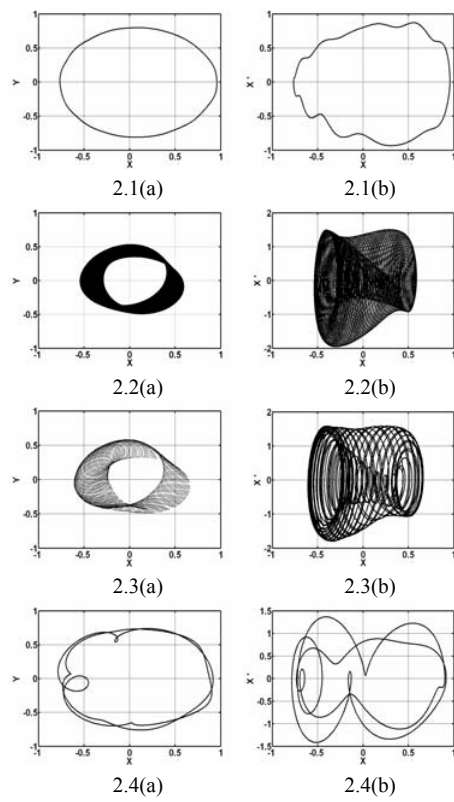


Fig. 2. Trajectories of rotor center at $m_r = 2.12, 3.48, 7.14$ and 10.79 kg (Figs. 2.1(a)-2.4(a)) and phase portraits (Figs. 2.1(b)-2.4(b)) (at $\omega = 1288$ rad/s).

speed. Table 2 summarizes the Poincaré data for the rotor center calculated by the DTM&FDM method with two different time step values, \tilde{H} . For both rotor mass and bearing number values, the results computed for the rotor center orbits using different time steps are in agreement to approximately 4 decimal places.

4.2 Dynamic analysis

Case I

The gas bearing is loaded with a rotational velocity of $\omega = 1288$ rad/s and the rotor mass m_r is chosen as the bifurcation parameter.

(a) Dynamic orbits and phase portraits

Figs. 2.1(a), .., 2.1(d) show that the dynamic orbit of the rotor center is regular at a low value of the rotor mass ($m_r = 2.12$ kg), but becomes irregular at $m_r = 3.48$ kg. At a rotor mass of $m_r = 3.54$ kg, the rotor center performs regular motion, but then performs irregular quasi-periodic motion as the rotor mass is further increased to $m_r = 7.14$ kg. Finally, at rotor mass values of $m_r = 10.79$ kg, the rotor center performs subharmonic-2T-periodic motion.

Figs. 2.2(a), .., 2.2(d) show the phase portraits of the rotor center at different values of the rotor mass. The phase portrait of the rotor center is symmetric and regular at $m_r = 2.12$ kg, but becomes irregular as the rotor mass is increased to $m_r = 3.48$

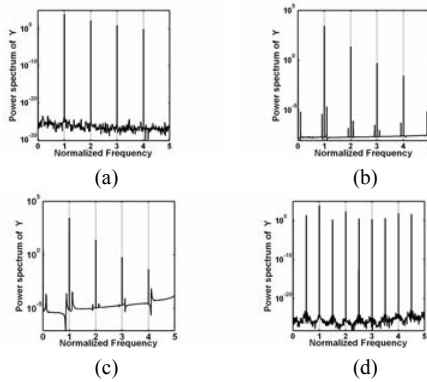


Fig. 3. Power spectra of rotor center in vertical direction at $m_r = 2.12$, 3.48 , 7.14 and 10.79 kg (at $\omega = 1288$ rad/s).

kg. At rotor mass values of $m_r = 7.14$ and 10.79 kg, the phase portraits are all non-symmetric and are more complicated than those at low values of the rotor mass.

(b) Power spectra

Figs. 3(a), ..., 3(d) show the dynamic response of the rotor center as a function of the rotor mass in the vertical direction. At a low rotor mass of $m_r = 2.12$ kg, the power spectra indicate that the rotor center performs T-periodic motion. When the rotor mass is increased to $m_r = 3.48$ kg, the rotor center motion transits to quasi-periodic motion in vertical direction (Figs. 3(b)). However, as the rotor mass is further increased to $m_r = 7.14$ kg, the rotor center performs quasi-periodic motion. Finally, at rotor mass values of $m_r = 10.79$ kg, the rotor center performs 2T sub-harmonic motion.

(c) Bifurcation diagrams and Poincaré maps

The bifurcation diagrams in Fig. 4 plot the rotor center displacement against the rotor mass m_r for values of m_r in the range 1.0 to 12.0 kg. Fig. 5 show the local bifurcations of the rotor center over the rotor mass ranges $3.0 \leq m_r \leq 4.0$ kg and $7.0 \leq m_r \leq 9.0$ kg, respectively. Meanwhile, Figs. 6(a)-6(d) present the Poincaré maps at $m_r = 2.12$, 3.48 , 7.14 and 10.79 kg, respectively. Observing Fig. 5(a), it is seen that the rotor center performs T-periodic motion at low values of the rotor mass, i.e. $m_r < 3.48$ kg. This is confirmed by the Poincaré map shown in Fig. 6(a) for a rotor mass of 2.12 kg. However, at $m_r = 3.48$ kg, the T-periodic motion transits to quasi-periodic motion (see Fig. 6(b)). From Fig. 5(a), it is seen that both quasi-periodic motion and T-periodic motion exist over the rotor mass range $3.48 \leq m_r < 3.59$ kg. As the rotor mass is increased from 3.59 kg to 8.09 kg, the rotor center performs quasi-periodic motion (see Fig. 5(b) and Fig. 6(c)) for $m_r = 7.14$ kg, for example. Figs. 4 and 5(b) show that this quasi-periodic motion reverts to T-periodic motion at $m_r = 8.1$ kg. However, at $m_r = 10.79$ kg, the T-periodic motion is replaced by 2T-periodic motion, as shown in Fig. 6(d). Fig. 4 shows that this 2T-periodic motion is maintained over the rotor mass interval $10.79 \leq m_r < 11.73$ kg, but reverts to T-periodic motion for rotor mass values in the range $11.73 \leq m_r < 12$ kg. Table 3

Table 3. Evolution of rotor center motion behavior over rotor mass interval $1.0 \leq m_r < 12$ kg.

Rotor mass (kg)	[1.0, 3.48)	[3.48,3.6)	[3.6,8.1)	[8.1,10.79)
Dynamic Behavior	T	T,Quasi (mixed)	Quasi	T
Rotor mass (kg)	[10.79,11.73)	[11.73,12.0)		
Dynamic Behavior	2T	T		

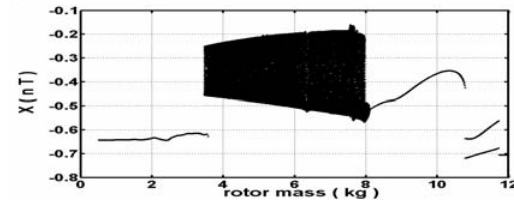


Fig. 4. Bifurcation diagrams versus rotor mass m_r at $\omega = 1288$ rad/s.

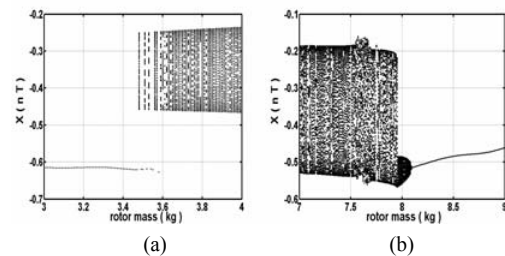


Fig. 5. Local bifurcation diagrams versus rotor mass m_r over interval (a) $3 \leq m_r \leq 4$ kg and (b) $7 \leq m_r \leq 9$ kg at $\omega = 1288$ rad/s.

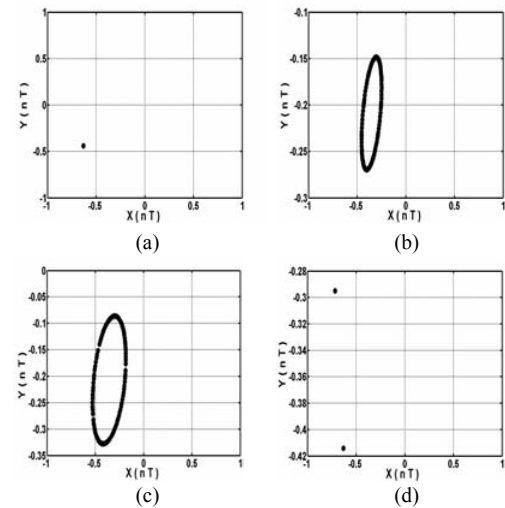


Fig. 6. Poincaré maps of rotor center trajectory at: (a) $m_r = 2.12$, (b) 3.48 , (c) 7.14 and (d) 10.79 kg.

summarizes the evolution of the rotor center motion behavior as the rotor mass is increased from $1 \leq m_r < 12$ kg.

Case II

In the second dynamic analysis case, the rotor mass is speci-

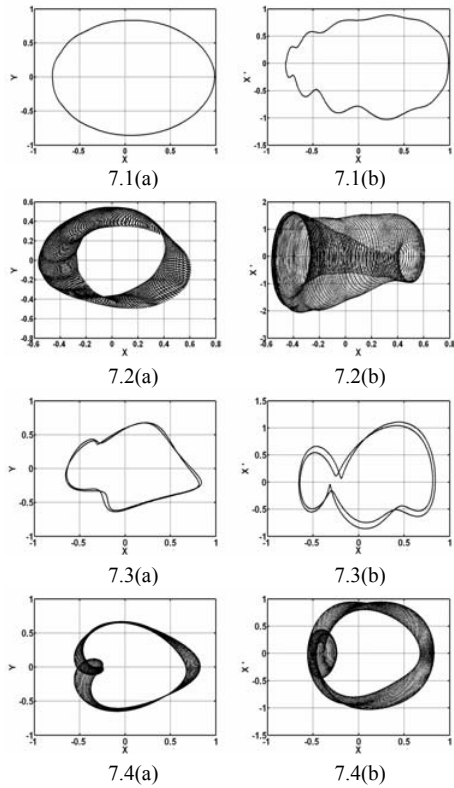


Fig. 7. Trajectories of rotor center at $\Lambda = 1.3, 1.82, 4.16$ and 6.43 (Figs. 7.1(a)-7.4(a)) and phase portraits (Figs. 7.1(b)-7.4(b)) (at $m_r = 3.2$ kg).

fied as $m_r = 3.2$ kg and the bearing number Λ is chosen as the bifurcation parameter.

(a) Dynamic orbits and phase portraits

Figs. 7.1(a), ..., 7.1(d) show that the orbits of the rotor center are regular at low bearing numbers (i.e. $\Lambda=1.3$), but become irregular at $\Lambda=1.82$. At higher bearing numbers of $\Lambda=4.16$ and 6.43 , the rotor center motion reverts to irregular, sub-harmonic and quasi-periodic motion, respectively.

Figs. 7.2(a), ..., 7.2(d) present the phase portraits of the rotor center at different values of the bearing number. The phase portrait is symmetric and regular at a bearing number of $\Lambda=1.3$, but becomes irregular, non-symmetric and non-periodic when the bearing number is increased to $\Lambda=1.82$. Finally, it is observed that the phase portraits are irregular at bearing numbers of $\Lambda = 4.16$, but are non-periodic and non-symmetric at a bearing number of $\Lambda=6.43$.

(b) Power spectra

Figs. 8(a), ..., 8(d) show the dynamic response of the rotor center as a function of the bearing number in the vertical direction. It is seen that the rotor center performs harmonic motion in both the horizontal and the vertical directions at a bearing number of $\Lambda=1.3$. However, when the bearing number is increased to $\Lambda=1.82$, the power spectra show that the rotor center exhibits quasi-periodic motion. As the bearing number is increased to $\Lambda=4.16$, the orbits transit to 2T-sub-harmonic motion. Finally, at $\Lambda=6.43$, the rotor motion reverts to quasi-

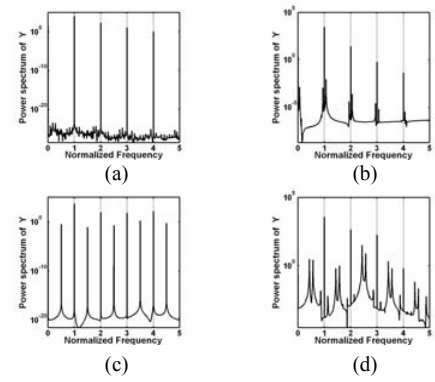


Fig. 8. Power spectra of rotor center in vertical direction $\Lambda = 1.3, 1.82, 4.16$ and 6.43 (at $m_r = 3.2$ kg).

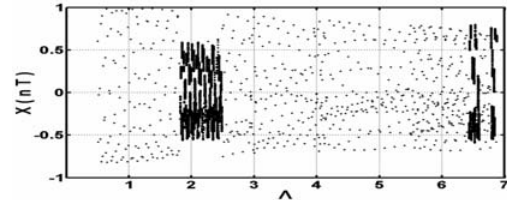


Fig. 9. Bifurcation diagrams versus bearing number Λ over interval $0.5 \leq \Lambda < 7$ at $m_r = 3.2$ kg.

periodic motion.

(c) Bifurcation diagrams and Poincaré maps

The bifurcation diagrams in Fig. 9 plot the rotor center displacement against the bearing number Λ over the range $0.5 \leq \Lambda < 7.0$. Figs. 10 show the local bifurcations of the rotor center over the bearing number range $1.6 \leq \Lambda \leq 2.8$ and $6.0 \leq \Lambda \leq 6.8$, respectively. Finally, Figs. 11(a)-11(d) plot the Poincaré maps of the rotor center trajectory at $\Lambda=1.3, 2.93, 6.43$ and 6.6 , respectively. At a low value of the bearing number ($\Lambda=1.3$), the rotor center performs T-periodic motion in both the horizontal and the vertical directions (see Fig. 11(a)). However, at $\Lambda=1.82$, the T-periodic motion becomes unstable and is replaced by quasi-periodic motion. Fig. 10(a) shows that the rotor center performs quasi-periodic motion at all values of the bearing number in the interval $1.82 \leq \Lambda < 2.49$ other than $\Lambda=2.26$ (T-periodic motion). As shown in Fig. 10(a), this quasi-periodic motion is replaced by T-periodic motion as the bearing number is increased from $\Lambda=2.49$ to 2.92 . However, at a bearing number of $\Lambda=2.93$, the T-periodic motion abruptly transits to 2T-periodic motion, as shown in Fig. 11(b). As the bearing number is increased over the range $2.93 \leq \Lambda < 3.03$, the rotor center performs 2T-periodic motion. As shown in Table 4, the evolution of the rotor center motion over the bearing number range $2.49 \leq \Lambda < 6.43$ can be summarized as follows: T-2T-T-2T-T-2T. Finally, as the bearing number is increased from $\Lambda=6.43$ to $\Lambda=7.0$, the rotor center motion evolves through the following behaviors: quasi-2T-quasi, as shown in Fig. 10(b) and Table 4. The Poincaré maps presented in Figs. 11(c) and 11(d) show that the rotor center performs quasi-periodic motion and 2T-

Table 4. Evolution of rotor center motion behavior over bearing number interval $0.5 \leq \Lambda < 7.0$.

Bearing number Λ	[0.5,1.82)	[1.82,2.49)	[2.49,2.93)	[2.93,3.03)
Dynamic Behavior	T	Quasi (except $\Lambda = 2.26, T$)	T	2T
Bearing number Λ	[3.03,3.95)	[3.95,4.16)	[4.16,5.52)	[5.52,6.43)
Dynamic Behavior	T	2T	T	2T
Bearing number Λ	[6.43,6.6)	[6.6,6.78)	[6.78,7.0)	
Dynamic Behavior	Quasi	2T	Quasi	

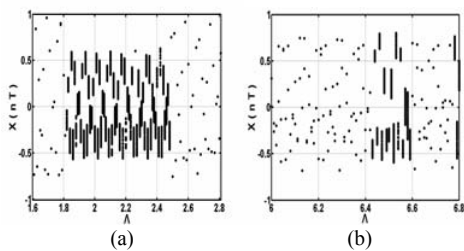


Fig. 10. Local bifurcation diagrams versus bearing number Λ over interval (a) $1.6 \leq \Lambda \leq 2.8$ and (b) $6.0 \leq \Lambda \leq 6.8$ at $m_r = 3.2$ kg.

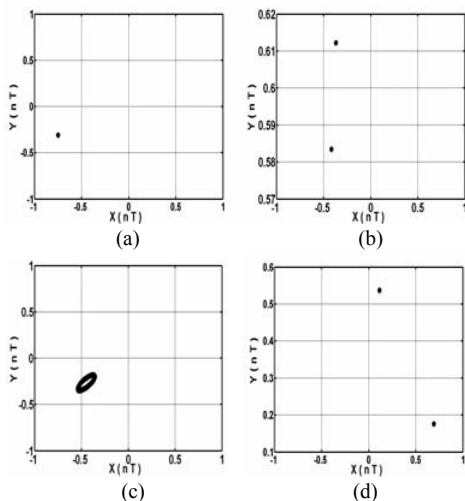


Fig. 11. Poincaré maps of rotor center trajectory at (a) $\Lambda = 1.3$, (b) 2.93 , (c) 6.43 and (d) 6.6 .

periodic motion at $\Lambda = 6.43$ and $\Lambda = 6.6$, respectively.

5. Conclusions

This paper has analyzed the nonlinear dynamic behavior of a rigid rotor supported by a relatively short spherical gas journal bearing system. The numerical results presented in this paper show that the DTM technique provides highly accurate predictions of the dynamic behavior of the spherical gas journal bearing system. Moreover, the computational time expended by the hybrid DTM&FDM method in deriving the

bifurcation diagram is around 1/3 that of the time required by the SOR&FDM method.

The dynamic behavior of the rigid rotor has been analyzed by inspecting the system state trajectories, the Poincaré maps, the power spectra and the bifurcation diagrams. Regarding the effect of the rotor mass on the behavior of the bearing system, it has been shown that at rotor mass values of $m_r = 2.12$ kg and 3.48 kg, the Poincaré maps have the form of a single point and a closed curve, respectively, indicating that the rotor center performs T-periodic and quasi-periodic motion, respectively. However, when performing quasi-periodic motion, the rotor response becomes non-periodic; particularly in the two rotor mass ranges $3.48 \leq m_r < 3.6$ kg and $3.6 \leq m_r < 8.1$ kg shown in Table 3. Regarding the effect of the bearing number on the behavior of the bearing system, it has been shown that the rotor center exhibits a non-periodic behavior when it performs quasi-periodic motion in the three ranges $1.82 \leq \Lambda < 2.48$, $6.43 \leq \Lambda < 6.59$ and $6.78 \leq \Lambda < 7.0$, shown in Table 4.

Overall, the results presented in this study provide general guidelines for the design of a relatively short spherical gas journal bearing system and indicate the operating conditions which suppress non-periodic motion and therefore prevent non-periodic behavior.

Acknowledgment

The financial support of this research by the National Science Council of the R.O.C. under Grant No. NSC-97-2221-E-269-022 is greatly appreciated.

Nomenclature

- | | |
|-------------|--|
| P | : Dimensionless gas pressure distribution |
| h | : Dimensionless gap between rotating shaft and bushing |
| P, H | : p and h following differential transformation |
| \tilde{H} | : Time step |

References

- [1] W. A. Gross and E. C. Zachmanaglo, Perturbation solutions for gas-lubricating films, *ASME Journal of Basic Engineering*, 83 (1961) 139-144.
- [2] J. I. Nikolajsen and R. Holmes, Investigation of squeeze-film isolators for the vibration control of a flexible rotor, *ASME Journal of Mechanical Science*, 21 (4) (1979) 247-252.
- [3] X. H. Li and D. L. Taylor, Nonsynchronous motion of squeeze-film damper systems, *ASME Journal of Tribology*, 109 (1987) 169-176.
- [4] F. F. Ehrich, High order subharmonic response of high speed rotor in bearing clearance, stress and reliability in design, *ASME Journal of Vibration and Acoustics*, 110 (1988) 9-16.
- [5] J. Y. Zhao, I. W. Linnett and L. J. Mclean, Subharmonic and quasi-periodic motion of an eccentric squeeze film damper-mounted rigid rotor, *ASME Journal of Vibration and Acoustics*,

- tics*, 116, (1994) 357-363.
- [6] G. Adiletta, A. R. Guido and C. Rossi, Chaotic motions of a rigid rotor in short journal bearings, *Nonlinear Dynamics*, 10 (1996) 251-269.
- [7] C. C. Wang, Nonlinear dynamic behavior and bifurcation analysis of a rigid rotor supported by a relatively short externally pressurized porous gas journal bearing system, *ACTA Mechanica*, 183 (2006) 41-60.
- [8] C. C. Wang, H. T. Yau, M. J. Jang and Y. L. Yeh, Theoretical analysis of the non-linear behavior of a flexible rotor supported by herringbone grooved gas journal bearings, *Tribology International*, 40 (2007) 533-541.
- [9] C. C. Wang, Theoretical and nonlinear behavior analysis of a flexible rotor supported by a relative short herringbone-grooved gas journal-bearing system, *Physica D-Nonlinear Phenomena*, 237 (2008) 2282-2295.
- [10] C. C. Wang, and H. T. Yau, Chaotic analysis and control of microcandilevers with PD feedback using differential trans-
- formation method, *International Journal of Nonlinear Sciences and Numerical Simulation*, 10 (2009) 425-444.



Cheng-Chi Wang received B.S., M.A., and Ph. D. degrees in Mechanical Engineering from National Cheng Kung University, Taiwan in 1996, 1998 and 2001, respectively. Research interests include: nano-micro mechanics, nonlinear dynamic analysis, nonlinear control and numerical simulation. From the year 2003 to 2006, he served as the assistant professor of Dept. of Automation and Control Engineering of Far East University, and from the year 2006 to 2009, he was the associate professor of Dept. of Mechanical Engineering of FEU. Now, he is the professor of Dept. of Mechanical Engineering of FEU.